UNIVERSITÀ
DI TRENTO

Department of Physics

Master degree in Physics

Chaos things

Graduant:
Manuel Bitto

Supervisor:
Leonardo Ricci

Co-supervisor:
Alessio Perinelli

24 October 2024

Contents

Introduction

Chapter 1

An electronic analog of the Burridge-Knopoff model

1.1 Mechanical Burridge-Knopoff model

The Burridge-Knopoff (BK) spring-block model [1] is a two-dimensional system of massive blocks lying on a rough horizontal surface. Each block is connected to its nearest neighbors by a set of springs, and linked by another spring to an upper horizontal ceiling moving with constant velocity with respect to the lower plate, as shown in Fig. 1.1.

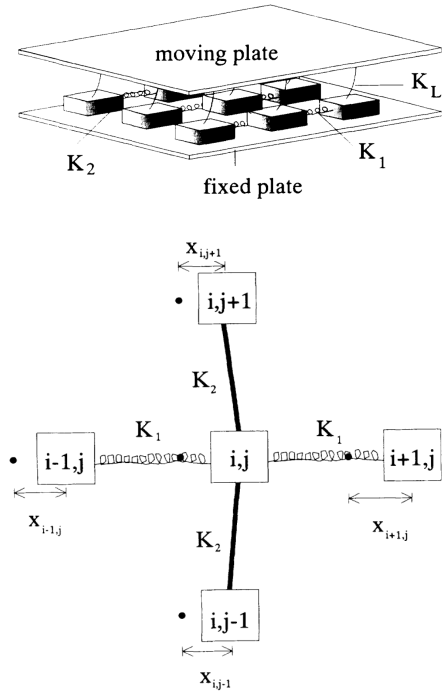

Figure 1.1: Visual representation of the Burridge-Knopoff spring-block model. K_1 and K_2 are the elastic constants, respectively, of the horizontal and vertical springs, while K_L is the elastic constant of the springs connecting the blocks and the moving plate. The figure below represents the interaction between a block and its four nearest neighbors, as a function of the displacement $x_{i,j}$. Figure adapted from Ref. [2].

The blocks are driven by the relative movement of the two rigid plates. When the force on one block reaches some threshold value F_{th}, the block slips, and it is reasonable to assume that the force on that block becomes zero. Then, the force on the four nearest neighbors is increased, often resulting in further slips, and an avalanche can occur.

The purpose of the BK model is the description of the dynamical behavior of real faults, whereby a constant, slow driving motion of plates produces an accumulation of "stress" up to a threshold at which such stress is released through an abrupt motion − i.e., an earthquake − of one or more of the system's constituent parts.

1.1.1 Motion of two coupled blocks

The mechanical BK model for the motion of two coupled blocks is shown schematically in Fig. 1.2. The upper ceiling moves with respect to the surface with a constant velocity u_d. Let x_1, x_2 be the displacements of the block positions relative to a state in which the springs are relaxed, and u_1, u_2 the velocities of the blocks in the lower surface frame, so that $u_i = u_d + \dot{x}_i$ with $i = 1, 2$.

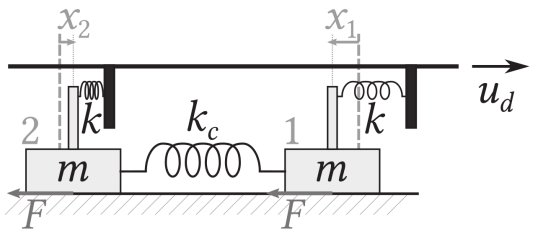

Figure 1.2: Two-blocks mechanical BK model. The upper ceiling, which the blocks are coupled to via springs with elastic constant k, is dragged with constant velocity u_d with respect to the underlying surface. This surface exerts a nonlinear, velocity-dependent friction F to each block's motion. Figure adapted from Ref. [3].

The equations of motion are thus given by

$$\begin{aligned} m\frac{\mathrm{d}u_1}{\mathrm{d}t} &= -kx_1 - k_c(x_1 - x_2) - F(u_1), \\ \frac{\mathrm{d}x_1}{\mathrm{d}t} &= u_1 - u_d, \\ m\frac{\mathrm{d}u_2}{\mathrm{d}t} &= -kx_2 - k_c(x_2 - x_1) - F(u_2), \\ \frac{\mathrm{d}x_2}{\mathrm{d}t} &= u_2 - u_d, \end{aligned} \tag{1.1}$$

where m is the mass of the blocks, k is the elastic constant of the springs that connect the blocks to the ceiling, k_c is the elastic constant of the spring linking the two blocks, and $F(u)$ is the nonlinear velocity-dependent friction. The velocities are assumed to be non-negative.

1.1.2 Dimensionless system

It is possible to render this system dimensionless by defining the following dimensionless quantities (i takes the values 1 and 2): a time $\tau \equiv t\sqrt{k/m}$, a velocity $\nu_i \equiv u_i/u_0$, a position $\xi_i \equiv x_i\sqrt{k/m}/u_0$, a friction $\varphi(\nu_i) \equiv F(\nu_i)/(u_0\sqrt{mk})$ and a parameter $\lambda \equiv k_c/k$. The four equations of motion can then be written as

$$\begin{aligned} \frac{\mathrm{d}\nu_i}{\mathrm{d}\tau} &= -(1+\lambda)\xi_i + \lambda\xi_{3-i} - \varphi(\nu_i), \\ \frac{\mathrm{d}\xi_i}{\mathrm{d}\tau} &= \nu_i - \nu_d. \end{aligned} \tag{1.2}$$

There exists a relative freedom in the choice of the friction $\varphi(\nu)$, provided that (i) $\varphi(\nu < 0) = 0$, (ii) $\varphi(\nu \geq 0) \geq 0$ and (iii) $\varphi(\nu)$ decreases down to zero from a maximum value $\varphi(0)$ that occurs at $\nu = 0$.

It is useful to define the equations of motion also in the case of a lower surface moving with a positive dimensionless velocity $\Delta\nu$, so that $\nu_i' = \nu_i + \Delta\nu$ and $\nu_d' = \nu_d + \Delta\nu$. The system of equations becomes:

$$\begin{aligned} \frac{\mathrm{d}\nu_i'}{\mathrm{d}\tau} &= -(1+\lambda)\xi_i + \lambda\xi_{3-i} - \varphi(\nu_i' - \Delta\nu), \\ \frac{\mathrm{d}\xi_i}{\mathrm{d}\tau} &= \nu_i' - \nu_d'. \end{aligned} \tag{1.3}$$

1.2 Electronic analog

In order to analyze the properties of the BK model, it is possible to build an electronic circuit which differential equations are the same as Eqs. 1.3. The first implementation was done by Field, Venturi and Nori [4] by drawing a direct parallelism between mechanical and electrical quantities. The idea was to use capacitance as mass, inductance as the reciprocal of elastic constant, voltage as velocity and current as position. However, this implementation has two main drawbacks. The first one is the usage of inductances, which are typically bulky and have intrinsically large tolerances compared with other components, resulting in higher uncertainties; moreover, their tunability is very low. The second issue is that the current is a state variable, and it is less straightforward to measure it with respect to voltage.

It is possible to use another implementation [3] which does not rely on inductances and uses only voltages as state variables. In order to do so it is necessary to rewrite the system equations as integral equations, so that they can be implemented by electronic integrators that are more stable than the differentiators. The new state variables are defined as $V_i \equiv \nu_i V_0$ and $W_i \equiv \xi_i V_0$ and the new time constant is given by $\tau = RC$, where R and C are suitably chosen resistance and capacitance. Integrating the system of Eqs. 1.3 for a moving surface and replacing $V_i' \equiv V_i + \Delta V$ and $V_d' \equiv V_d + \Delta V$,

where $V_d \equiv V_0 \nu_d$ and $\Delta V \equiv V_0 \Delta\nu$, leads to the following system of equations:

$$V_i + \Delta V = -\frac{1}{RC}\int \left[(1+\lambda)W_i - \lambda W_{3-i} + V_0 \varphi\left(\frac{V_i}{V_0}\right)\right] \mathrm{d}t,$$
$$W_i = -\frac{1}{RC}\int (V_d - V_i)\,\mathrm{d}t, \tag{1.4}$$

where $\lambda = R/R_c$ and R_c is a suitably chosen resistance.

These differential equations are implemented by the circuit shown in Fig. 1.4, which makes use of resistors, capacitors, diodes and operational amplifiers, without any inductance. Assuming for a while that ΔV and the nonlinear element $\varphi(V_i/V_0)$ were not present, the two integrations above could be promptly implemented by considering the black part of the circuit diagram. The blue part refers thus to the nonlinear element, while the red part is a standard inverting operational amplifier, which is necessary for the coupling between two blocks.

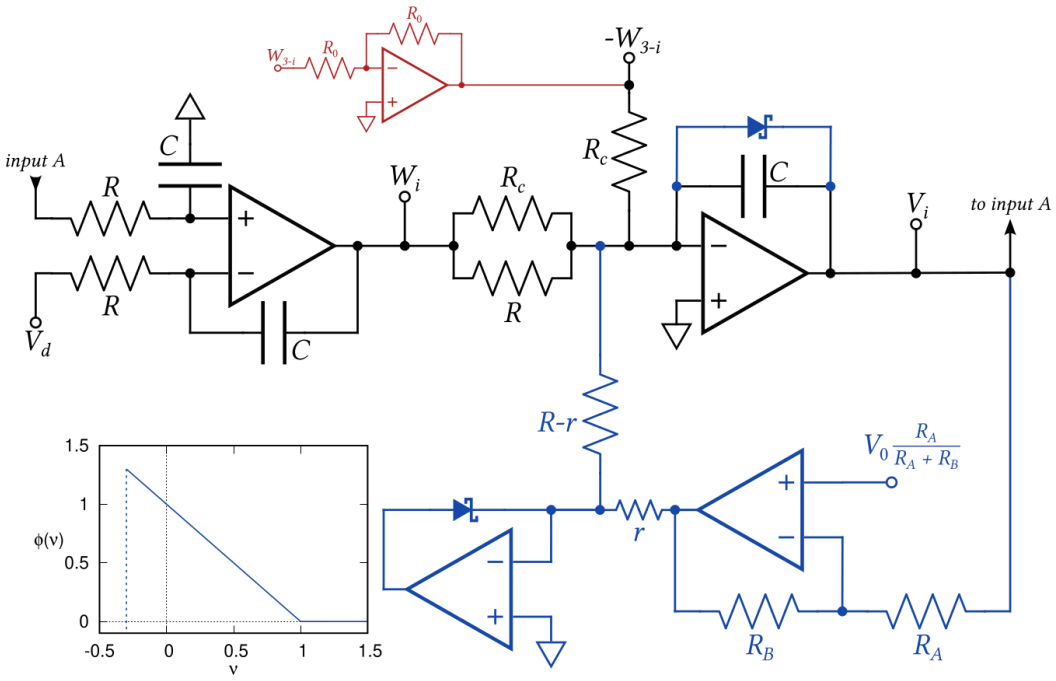

Figure 1.3: Inductorless representation of the BK model. The circuit diagram refers to a single block, labeled by $i = 1, 2$. The bottom left plot shows the characteristic of the nonlinear element, i.e. the blue part of the diagram. Figure adapted from Ref. [3].

1.3 Breadboard implementation

The inductorless electronic analog of the Burridge-Knopoff model [3] is represented in Fig. 1.4. This circuit was implemented in a breadboard using 1N5817 Schottky diodes and different kinds of op-amps, namely UA741, OP07, TL081 and OP27; these op-amps were supplied with $V_{CC} = \pm 12$ V. The nominal values for the resistances and capacitors are $R = R_c = 10$ kΩ, $R_A = R_B = 10$ kΩ, $r = 1.8$ kΩ and $C = 100$ nF.

The input voltages are $V_0 = 1$ V and the variable voltage V_d, while the output voltages are V and W (the subscript i is omitted).

The oscillating behavior of this circuit is shown in Fig. 1.5. The lower clamping in the Lissajous figure is intended and is due to the presence of the Schottky diodes. The frequency behavior at high voltages, namely $V_d \gtrsim 1$ V, is the same for each kind of op-amp. On the other hand, the amplitudes possess an offset which depends on the selected op-amp; nonetheless, they all exhibit a mostly linear behavior.

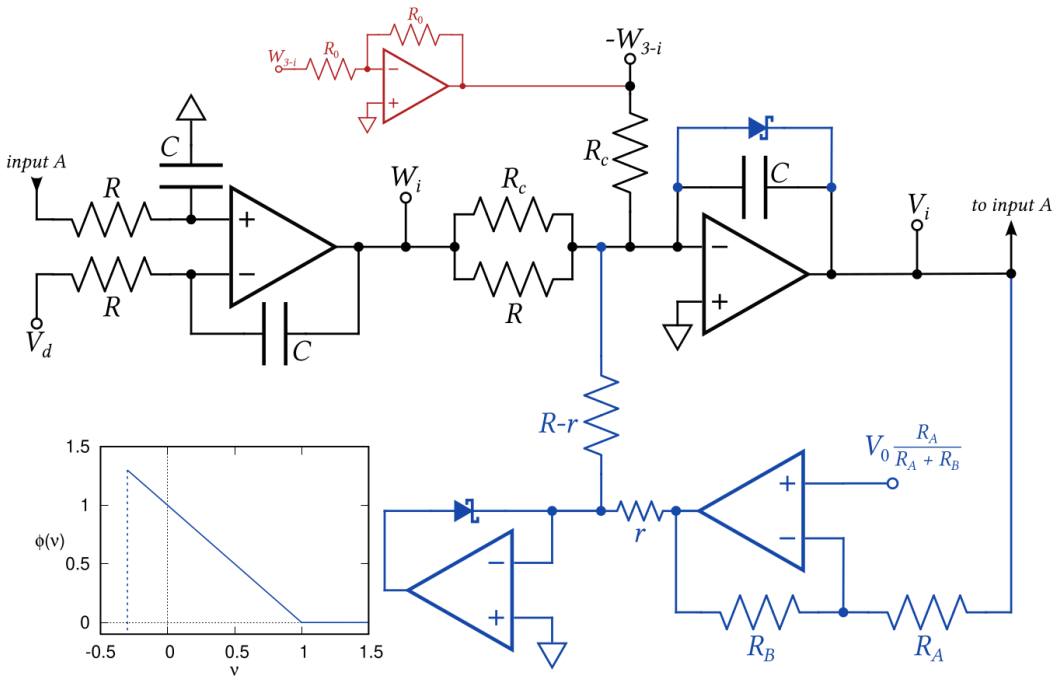

Figure 1.4: Inductorless representation of the BK model. The blue part of the network refers to the nonlinear element, whose characteristic is drawn in the bottom left plot. Figure adapted from Ref. [3].

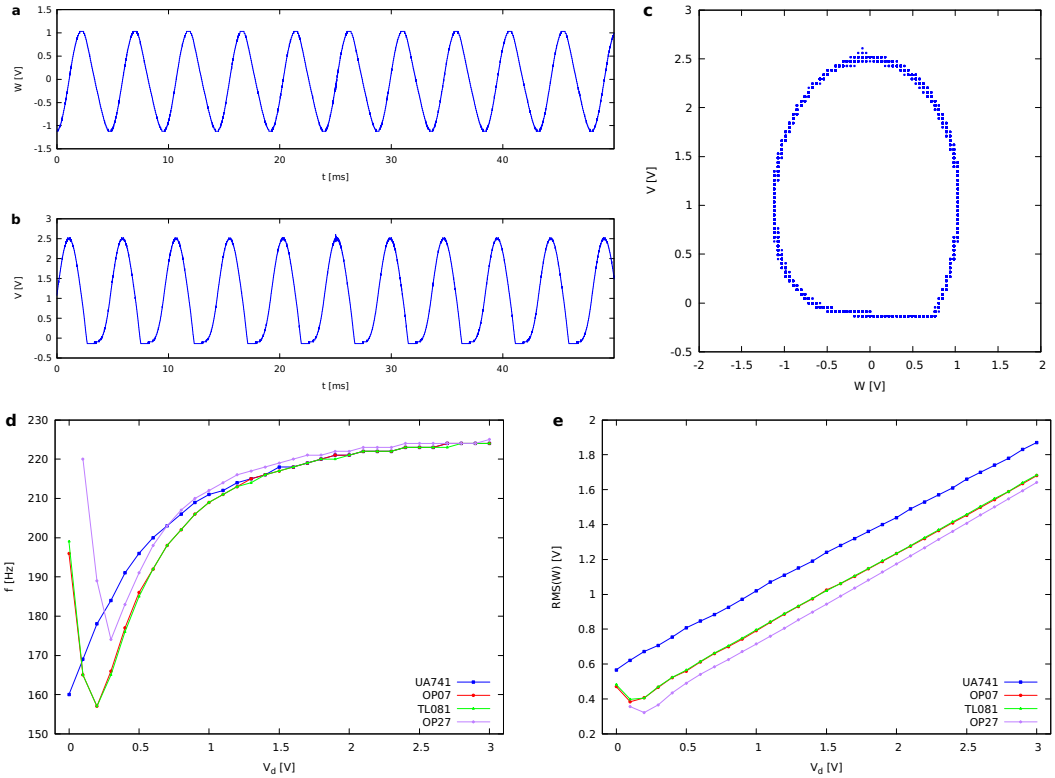

Figure 1.5: Oscillating behavior for the circuit implemented on the breadboard. (a) Plot of W and (b) of V as a function of time, for $V_d = 1$ V. (c) Phase portrait (Lissajous figure) of V versus W. (d) Frequency and (e) root mean square amplitude of the output signal W as a function of the parameter V_d and for different kinds of op-amps.

1.4 Prototypes

In order to describe the coupling between many oscillators it is not possible use the breadboard implementation of the circuit shown in Fig. 1.4, due to scalability issues. For the purpose of improving the system scalability, two smaller prototypical chips have been built. The circuit implemented in each chip is shown in Fig. 1.6. The differences between this circuit and the one used in the previous section lie in the nonlinear elements; in this case MBRA210L Schottky diodes have been used, as well as quad operational amplifiers OP470, which offer comparable performance to OP27 op-amps.

The oscillating behavior of this circuit is shown in Fig. 1.7 for both chips. These systems are much less stable with respect to the circuit implemented on the breadboard; in fact, measurements were possible only in a small range for V_d, namely $V_d \leq 1.1$ V for one chip and $V_d \leq 0.6$ V for the other one. It is also important to point out that the diode clamping is not present; in fact, it is only noticeable at voltages $V_d \lesssim 0.4$ V.

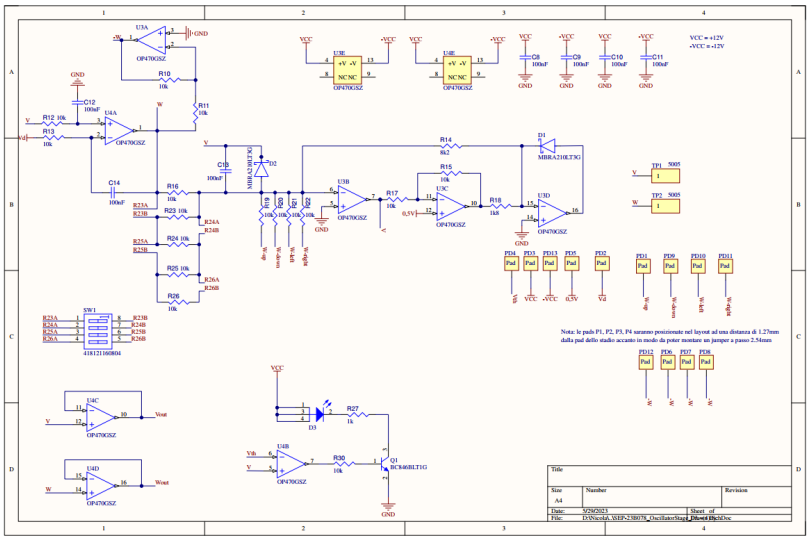

Figure 1.6: Circuit diagram of one prototypical chip.

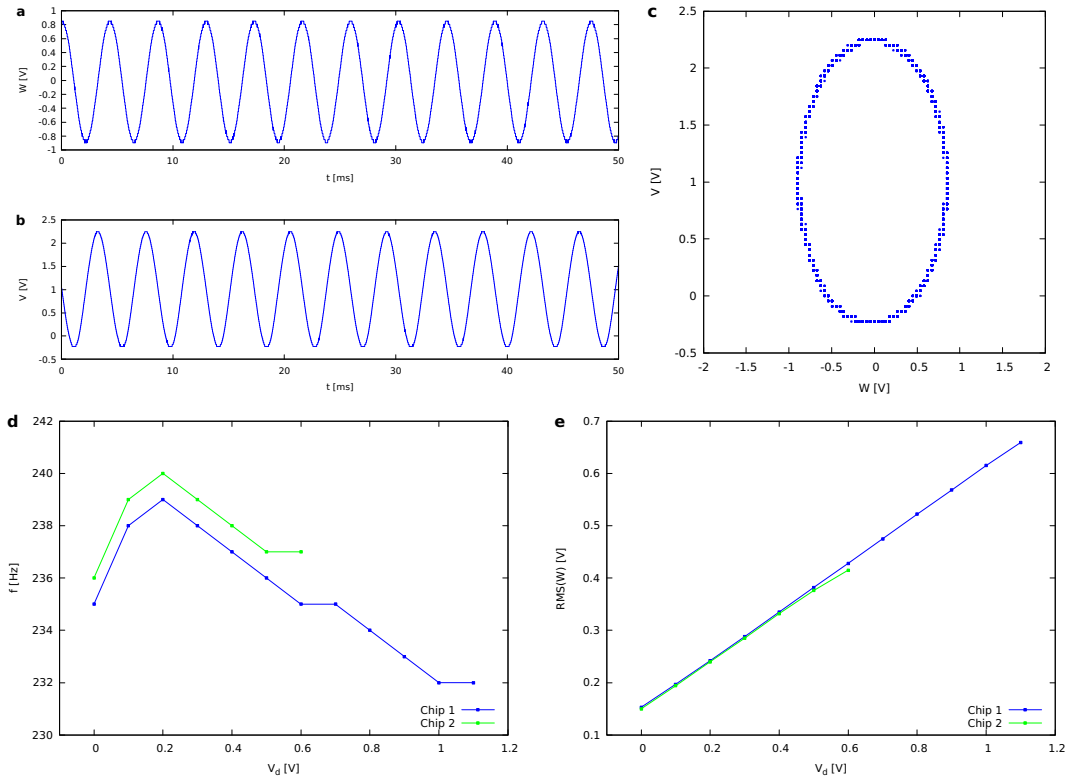

Figure 1.7: Oscillating behavior for the circuit implemented on the prototypical chips. (a) Plot of W and (b) of V as a function of time, for $V_d = 1$ V. (c) Phase portrait (Lissajous figure) of V versus W. (d) Frequency and (e) root mean square amplitude of the output signal W as a function of the parameter V_d and for the two different chips.

1.5 Board

In order to finally analyze the behavior of many coupled oscillators, a board containing 25 chips (or blocks) has been built. The circuit diagram is equivalent to the one shown in Fig. 1.6 for the prototypes, the only difference being the use of DFLS1100 Schottky diodes instead of MBRA210L ones.

The oscillating behavior is shown in Fig. 1.8. Once again, these systems are not as stable as the circuit on the breadboard; measurements were in fact taken for $V_d \leq 2.2$ V for the first two blocks. It is important to notice that in the voltage range 0.6 V $\leq V_d \leq$ 2.1 V a clamping of the output voltage V can be observed; this is not intended and is probably due to intrinsic limitations in the current.

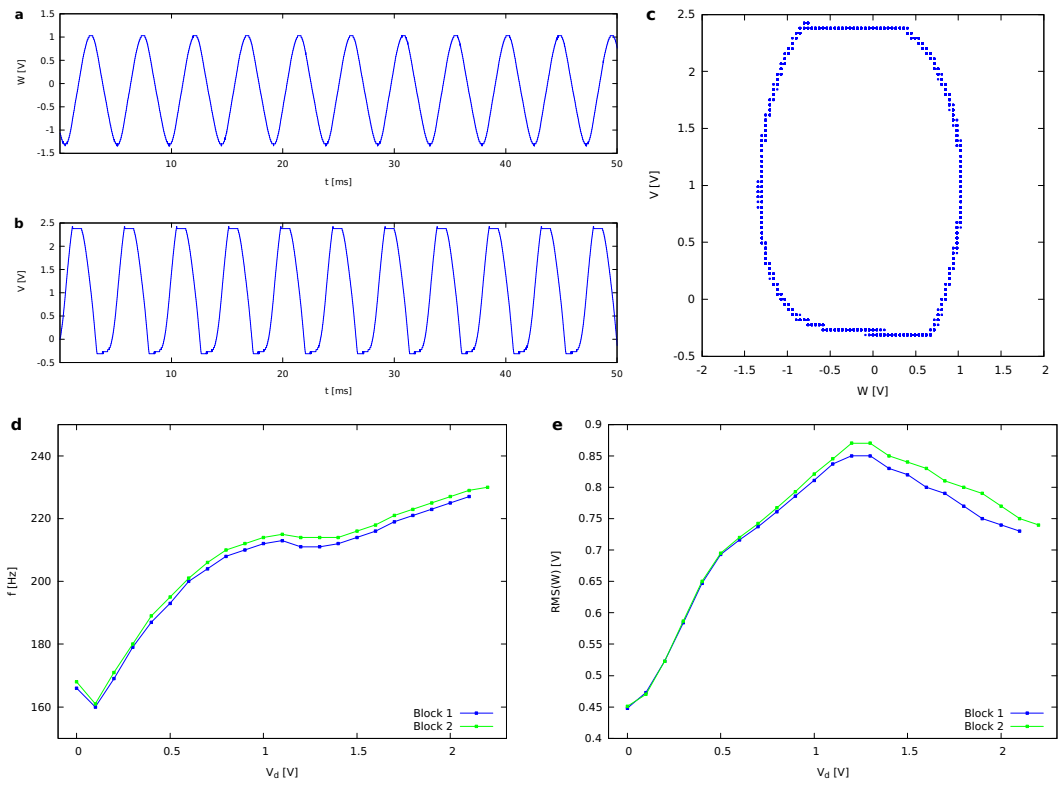

Figure 1.8: Oscillating behavior for the circuit implemented on the board. (a) Plot of W and (b) of V as a function of time, for $V_d = 1$ V. (c) Phase portrait (Lissajous figure) of V versus W. (d) Frequency and (e) root mean square amplitude of the output signal W as a function of the parameter V_d and for two different blocks.

1.6 New board

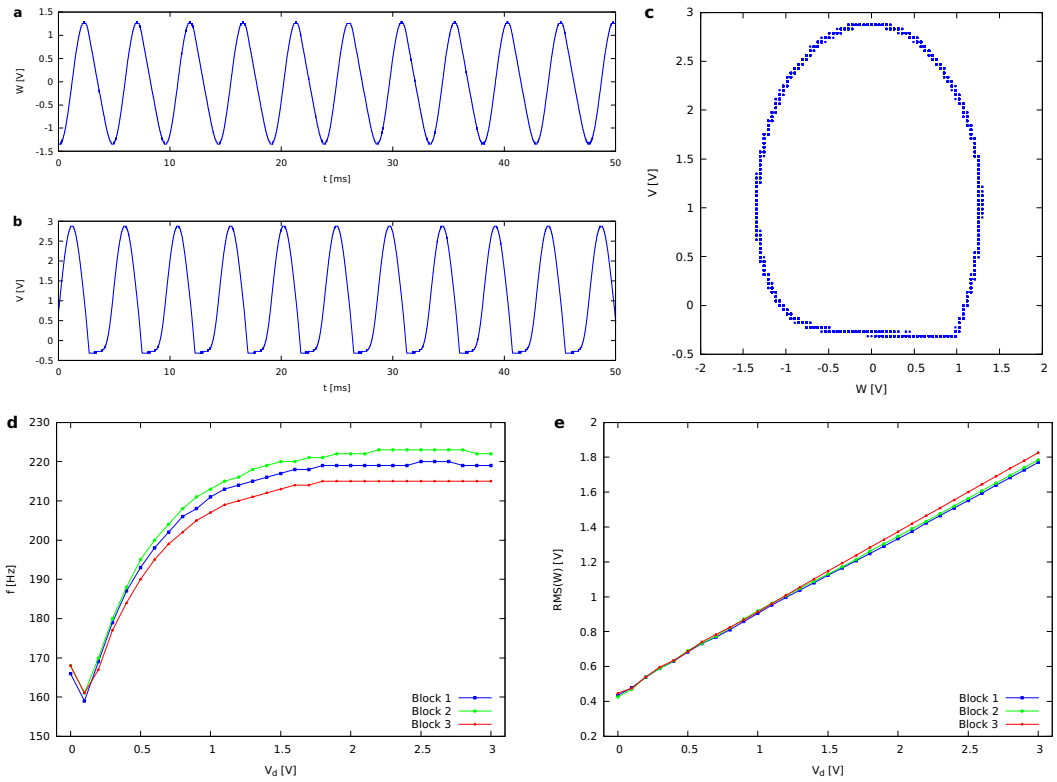

Figure 1.9: Oscillating behavior for the circuit implemented on the new board. (a) Plot of W and (b) of V as a function of time, for $V_d = 1$ V. (c) Phase portrait (Lissajous figure) of V versus W. (d) Frequency and (e) root mean square amplitude of the output signal W as a function of the parameter V_d and for three different blocks.

1.7 Conclusions

The comparison between frequency and amplitude on the three implementations is shown in Fig. 1.10. The frequency of the board is very similar to the breadboard one for voltages $V_d < 1$ V; at higher voltages there are small deviations in the board, probably due to the increased relevance of the current clamping. This might also be the reason why the amplitude behavior of the board is not linear.

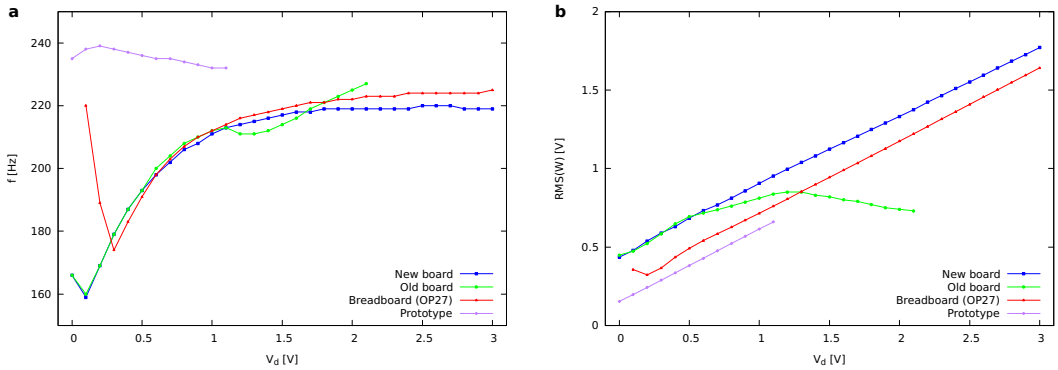

Figure 1.10: (a) Frequency and (b) root mean square amplitude of the output signal W as a function of the parameter V_d for the three implementations of the BK model, i.e. the first block of the board, the breadboard implementation with the OP27 op-amps and the first prototypical chip.

Chapter 2

Chaos analysis of multiple oscillators

2.1 Two blocks

The coupling between two oscillators is performed by connecting the inverted voltage $-W_2$ of the second oscillator to the first one and viceversa, as shown in Fig. 1.4. A chaotic behavior can be observed, as can be seen in Fig. 2.1.

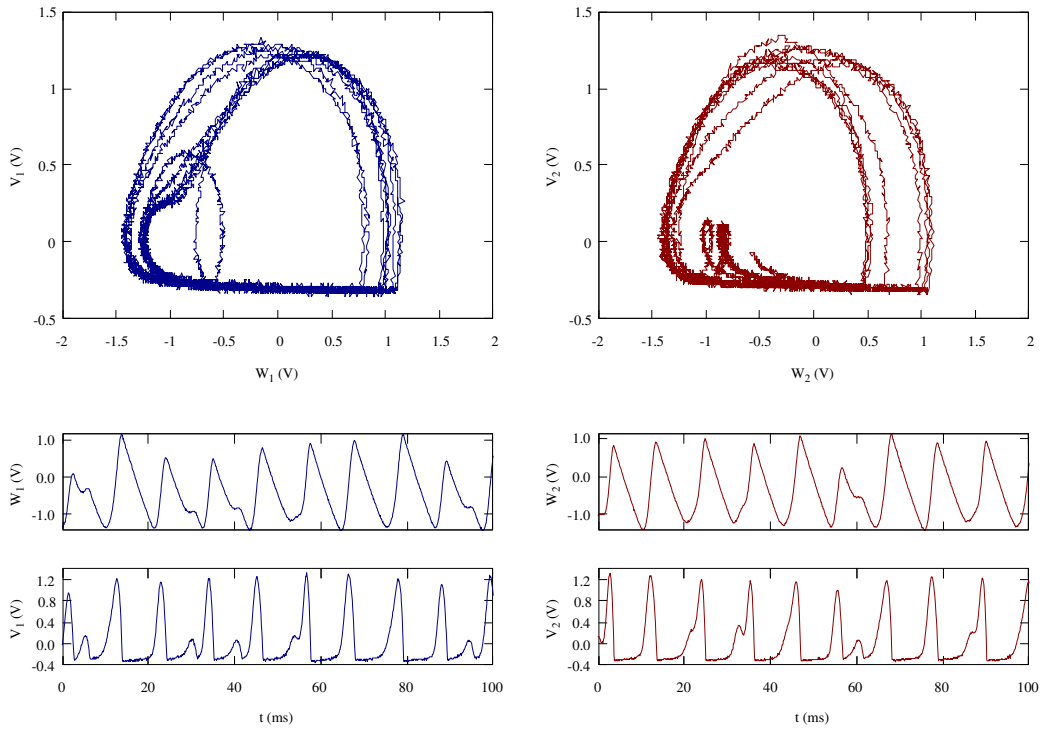

Figure 2.1: Chaotic behavior of two coupled blocks for $V_d = 0.05$ V and for a total time of 100 ms. Phase portraits of V_i vs W_i for the first (a) and second (b) block. Time series plots for W_1 (c), V_1 (e), W_2 (d) and V_2 (f).

In order to quantify the degree of chaos of this system, it is possible to carry out

an analysis

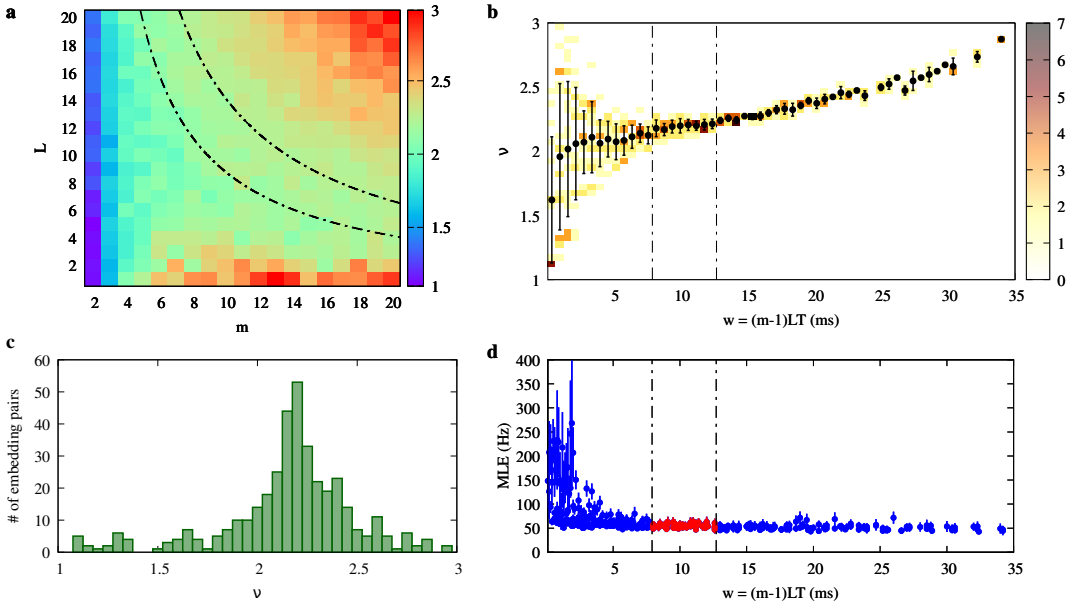

Figure 2.2: Edge

2.2 Three blocks

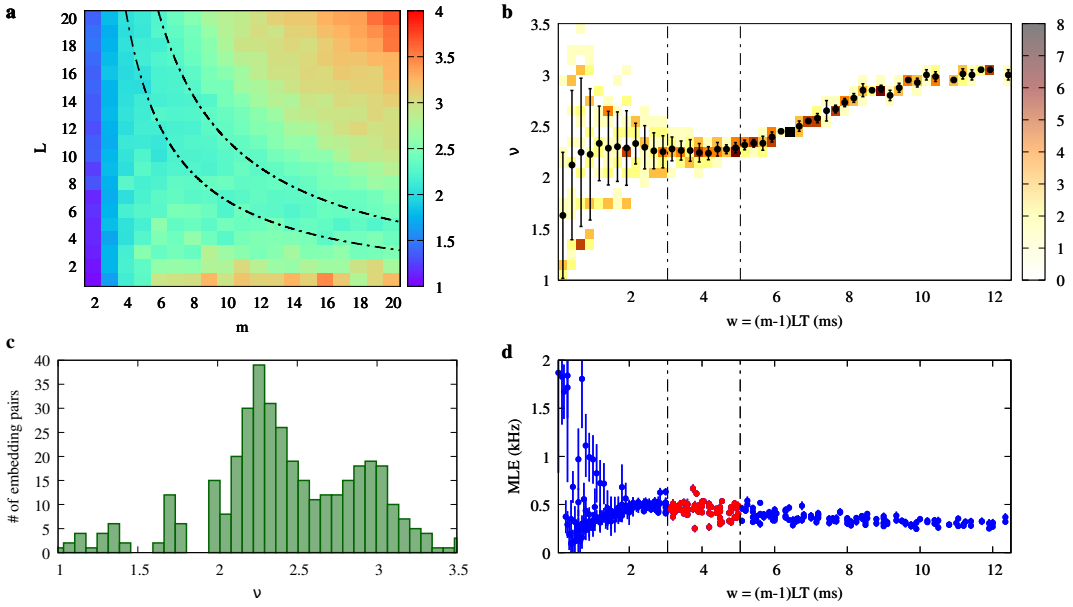

Figure 2.3: Edge

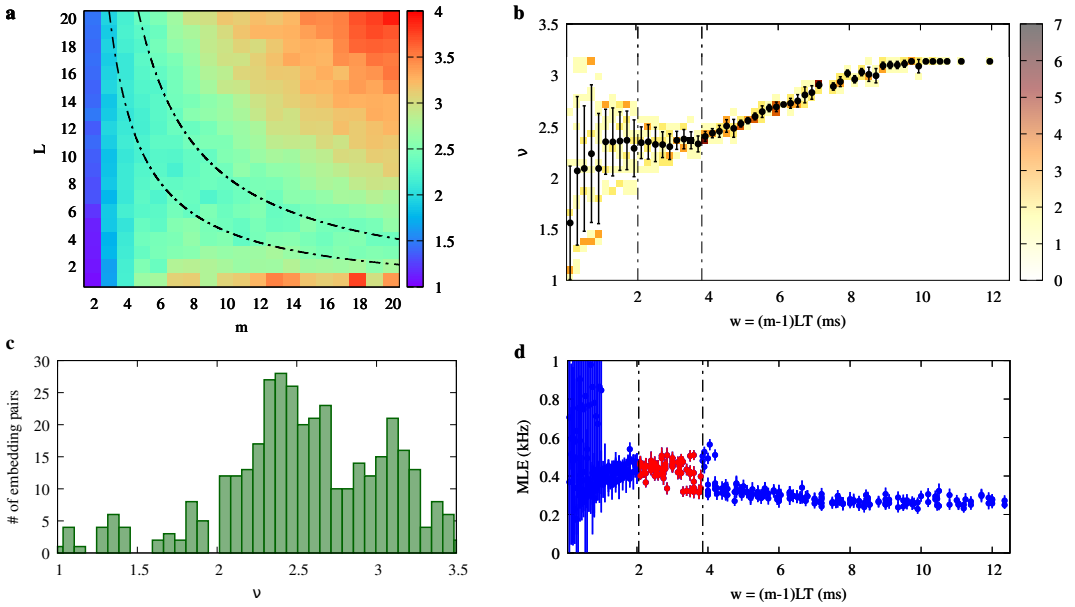

Figure 2.4: Middle

2.3 Four blocks

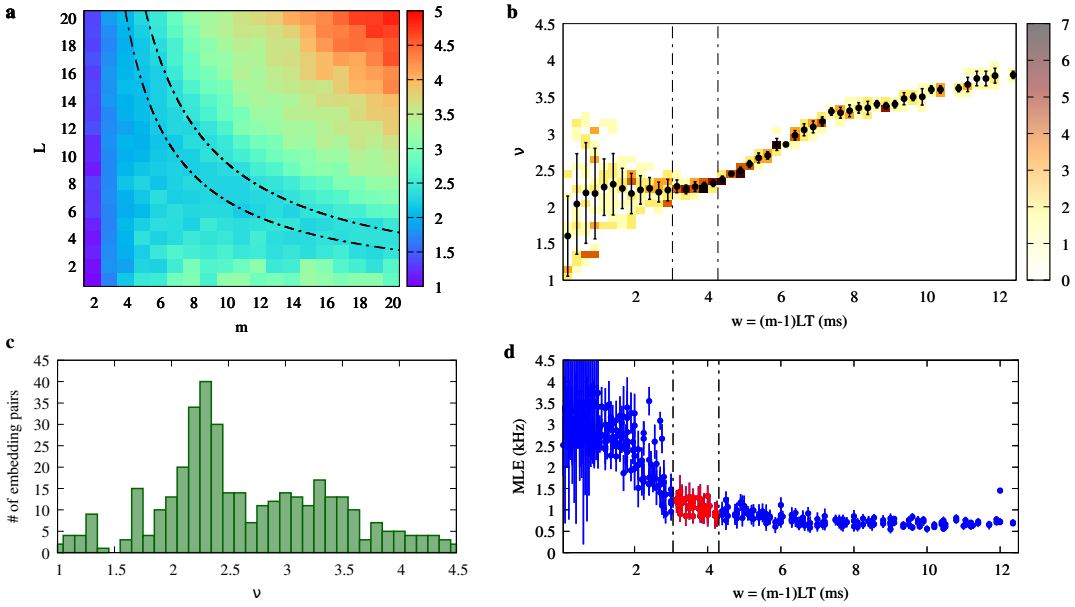

Figure 2.5: Edge

2.4 Five blocks

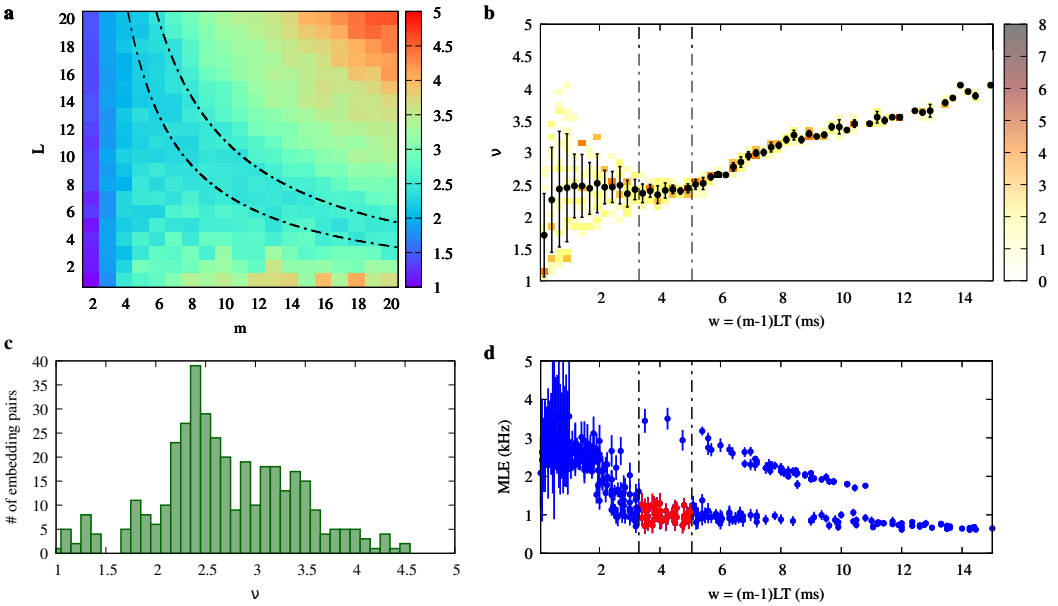

Figure 2.6: Edge

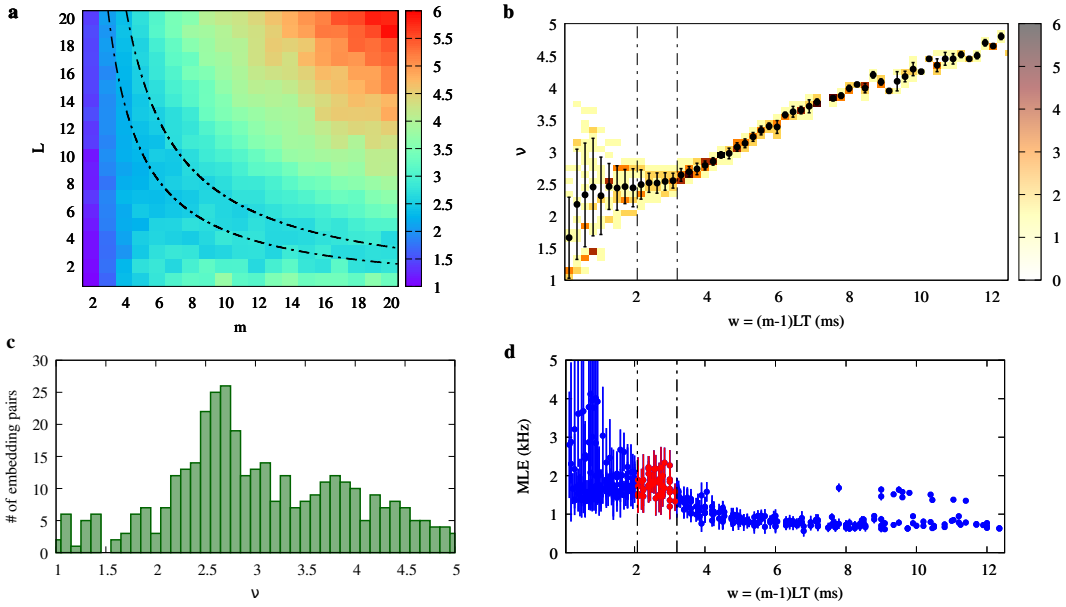

Figure 2.7: Middle

2.5 Six blocks

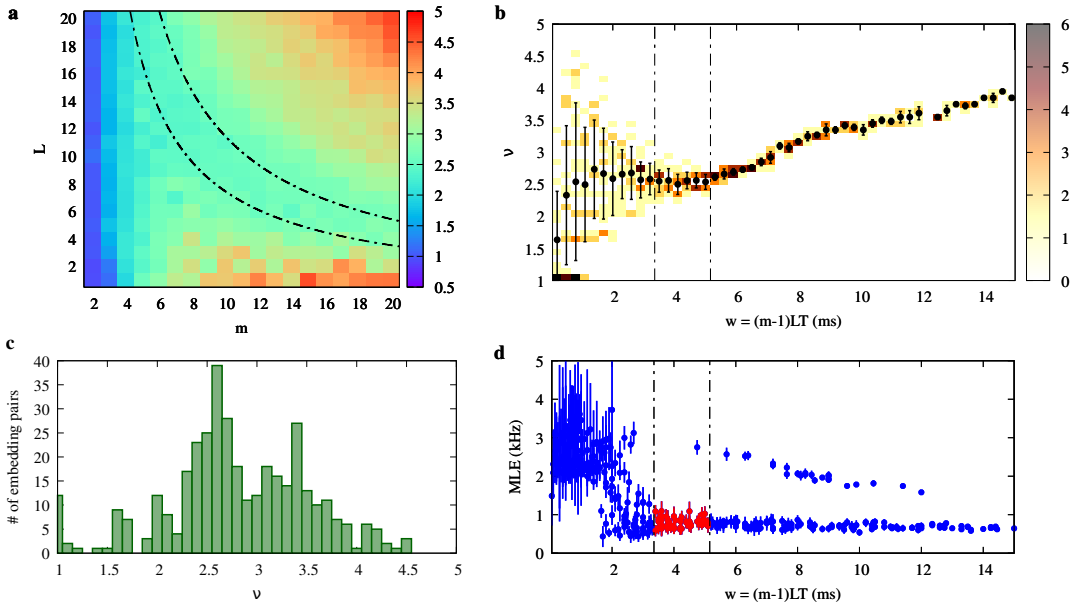

Figure 2.8: Edge

2.6 Seven blocks

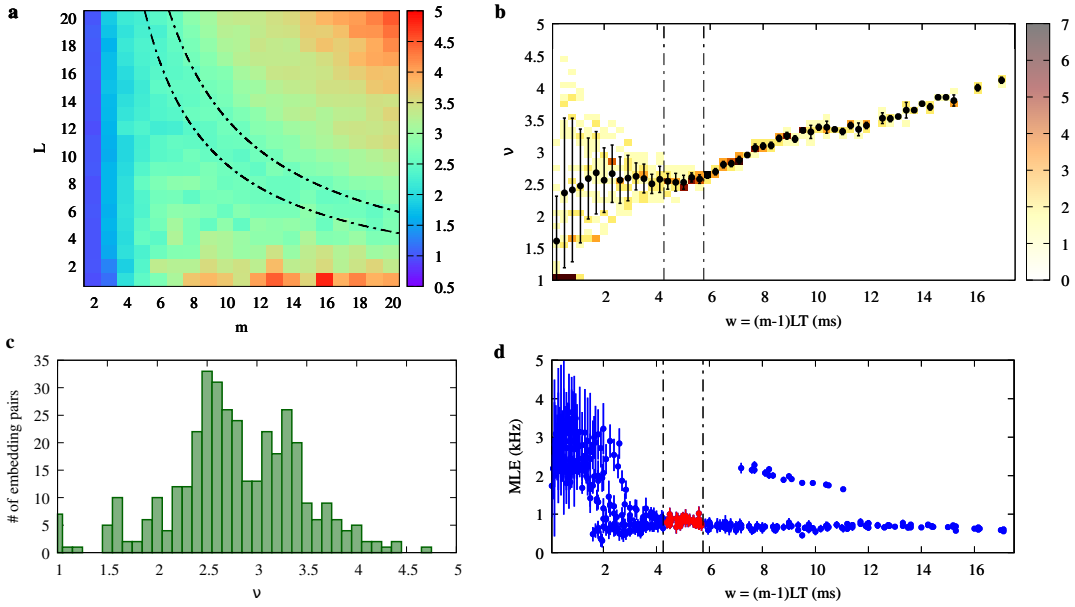

Figure 2.9: Edge

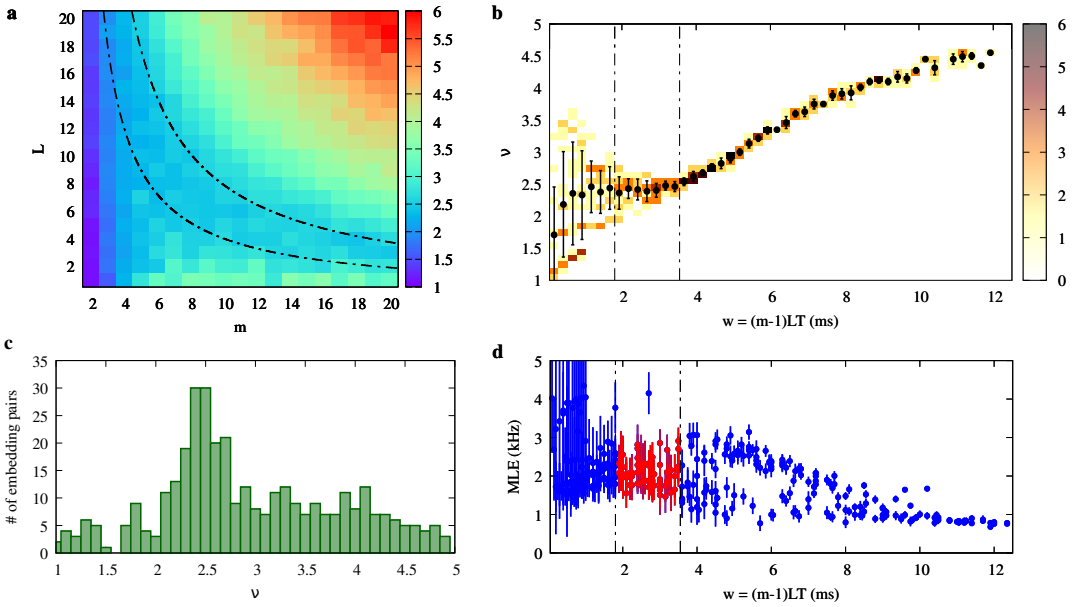

Figure 2.10: Middle

2.7 Eight blocks

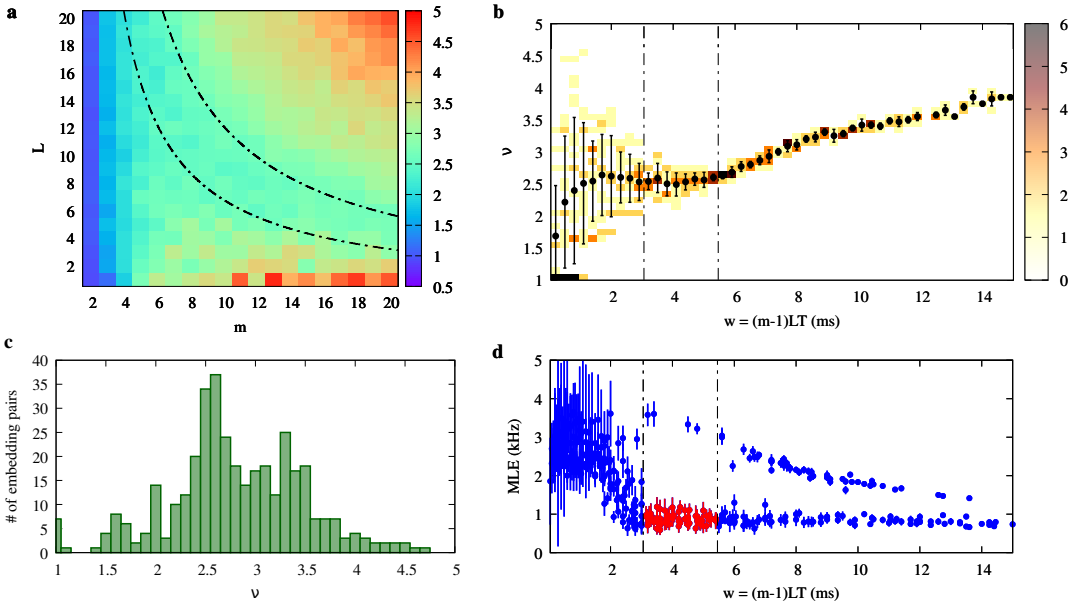

Figure 2.11: Edge

2.8 Nine blocks

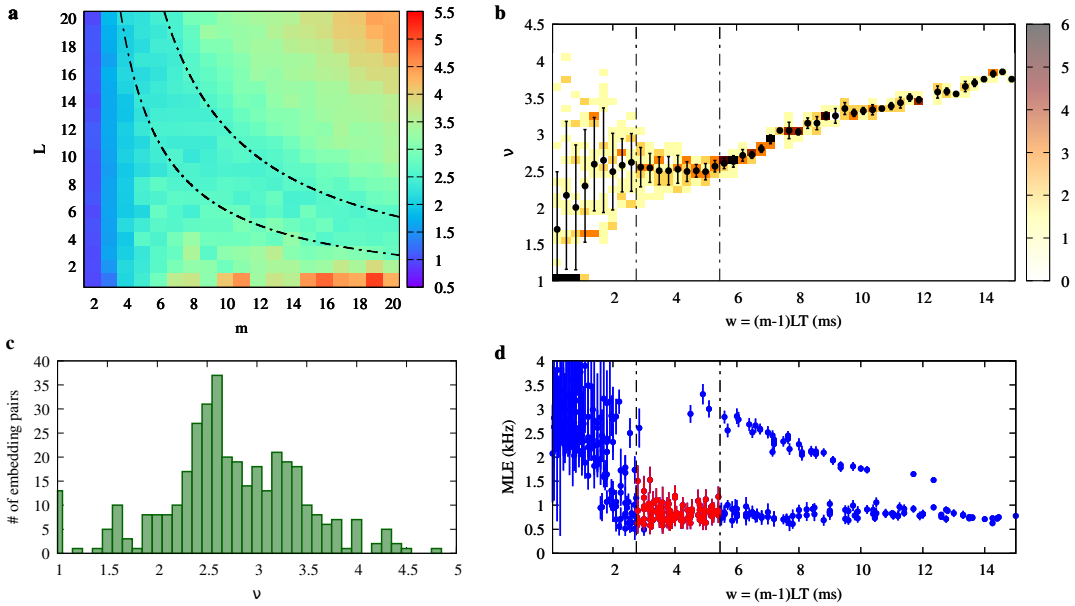

Figure 2.12: Edge

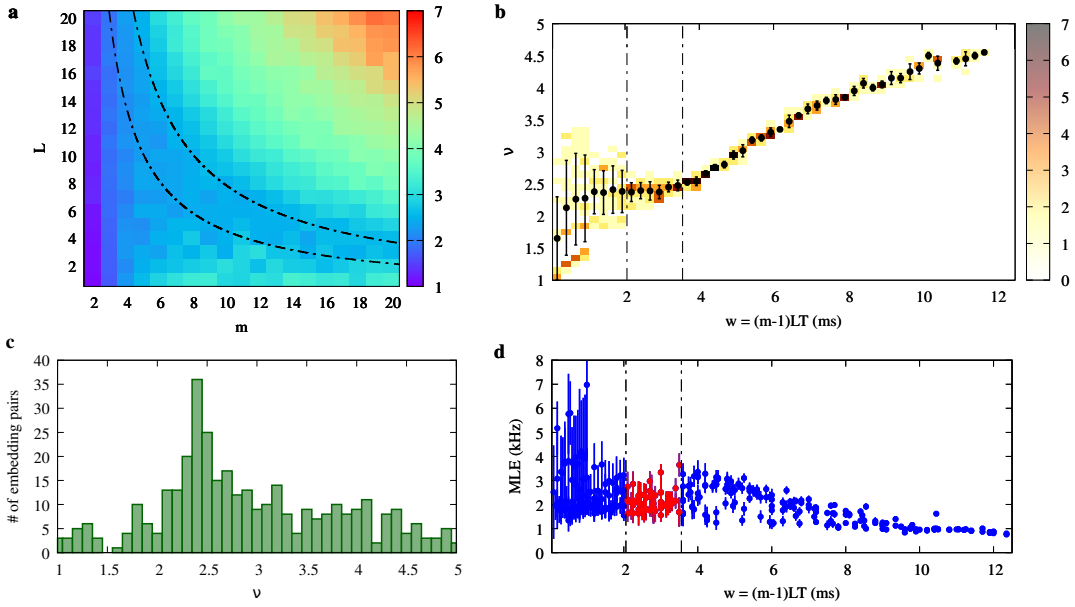

Figure 2.13: Middle

2.9 Ten blocks

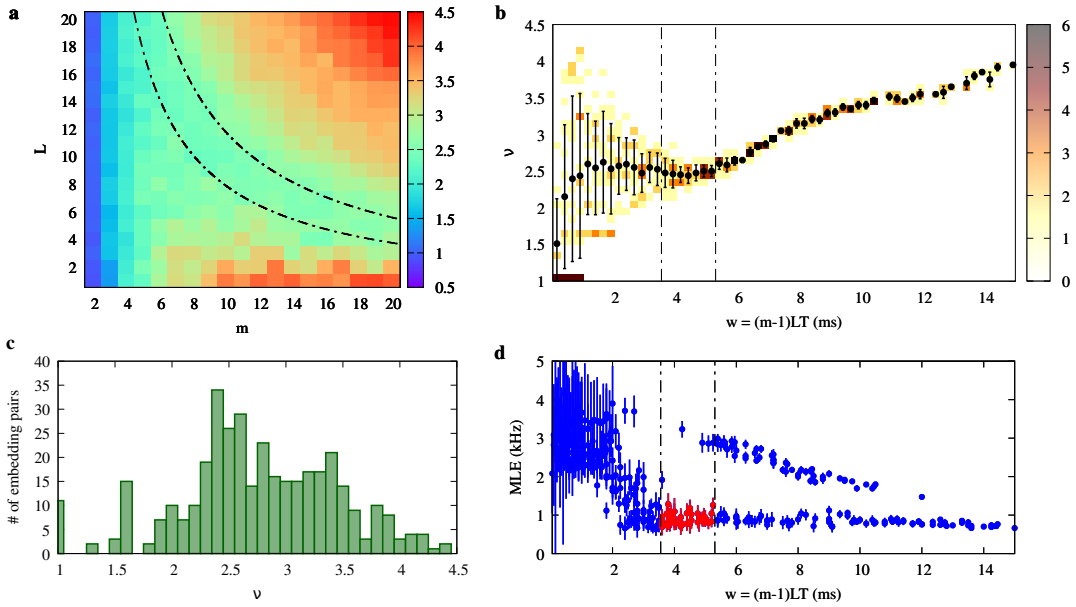

Figure 2.14: Edge

2.10 Conclusions

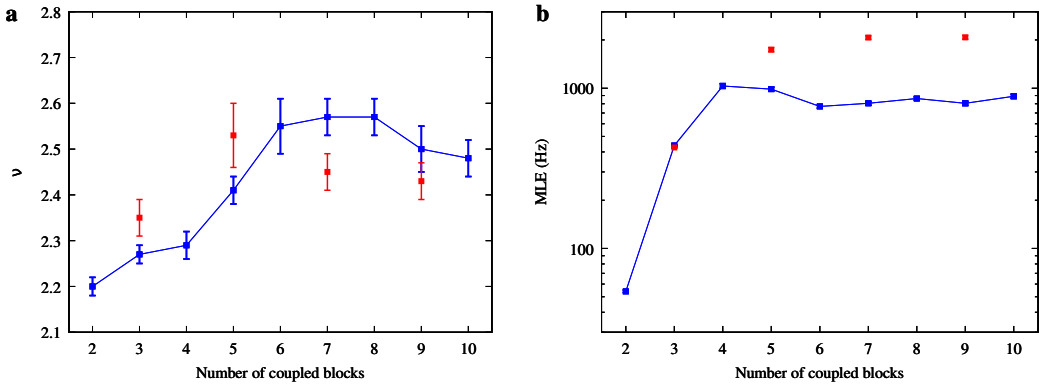

Figure 2.15: Edge (blue) and middle (red)

Chapter 3

Earthquake properties and statistical model of a fault

Bibliography

[1] R. Burridge and L. Knopoff. "Model and theoretical seismicity". In: *Bulletin of the Seismological Society of America* (1967).

[2] Zeev Olami, Hans Jacob S. Feder, and Kim Christensen. "Self-organized criticality in a continuous, nonconservative cellular automaton modeling earthquakes". In: *Phys. Rev. Lett. 68, 1244* (1992).

[3] A. Perinelli, R. Iuppa, and L. Ricci. "A scalable electronic analog of the Burridge–Knopoff model of earthquake faults". In: *Chaos 33, 093103* (2023).

[4] S. Field, N. Venturi, and F. Nori. "Marginal Stability and Chaos in Coupled Faults Modeled by Nonlinear Circuits". In: *Phys. Rev. Lett. 74* (1995).